The Global Distribution of Atmospheric Eddy Length Scales

ELIZABETH A. BARNES AND DENNIS L. HARTMANN

Department of Atmospheric Sciences, University of Washington, Seattle, Washington

(Manuscript received 13 June 2011, in final form 11 November 2011)

ABSTRACT

The correlation lengths of vorticity anomalies from temporal averages are examined in the 40-yr European Centre for Medium-Range Weather Forecasts Re-Analysis dataset. It is shown that, in the annual mean, eddies in the Southern Hemisphere are significantly larger than those in the Northern Hemisphere. The eddy vorticity lengths exhibit a strong seasonal cycle, with the largest scales occurring in the winter season. The maximum zonal eddy lengths closely follow the contours of the strong upper-level winds, while the maximum meridional lengths are found in jet exit regions and in the stratosphere.

1. Introduction

Eddies play an important role in defining the large-scale circulation, and their scale predominantly determines their propagation and dissipation (Hoskins et al. 1983). Kidston et al. (2010) demonstrated that the Coupled Model Intercomparison Project phase 3 (CMIP3) general circulation models (Meehl et al. 2007) exhibit a robust increase in zonal eddy length scale in future climates, and they suggest that this increase contributes to the predicted poleward migration of the midlatitude jets with increased greenhouse gases. Barnes and Hartmann (2011) present an alternative possibility, demonstrating that a poleward shift of the midlatitude jet can cause an increase in eddy size in a barotropic model, consistent with spherical Rossby wave theory.

Understanding eddy scales is clearly important to understanding future atmospheric circulation changes and pinpointing cause and effect. Chang and Yu (1999) and Chang (1999) performed in-depth studies of wave packets at 300 mb (hPa) in the midlatitudes with a focus on propagation characteristics of zonally propagating storm track disturbances (e.g., phase speed, period, group velocity estimations). Here, our focus is purely one of eddy scale throughout the atmosphere, and we present a three-dimensional picture of observed eddy vorticity scales as a reference point for understanding eddy scales more completely.

Corresponding author address: Elizabeth A. Barnes, Department of Atmospheric Sciences, University of Washington, Box 351640, Seattle, WA 98195.
E-mail: eabarnes@atmos.washington.edu

DOI: 10.1175/JCLI-D-11-00331.1

2. Data

The data consist of 44 years (1958–2001) of 2.5° × 2.5° latitude–longitude gridded daily (1200 UTC) relative vorticity and zonal wind from the 40-yr European Centre for Medium-Range Weather Forecasts (ECMWF) Re-Analysis (ERA-40) (Uppala et al. 2005).

We denote daily anomalies as $(\cdots)'$, and they are calculated by first subtracting the mean seasonal cycle at each grid point. The mean seasonal cycle is a smooth curve computed as the climatological mean plus the first four Fourier harmonics of the daily climatology for all seasons over the 44 years of data. Finally, to remove interannual variability, we remove the individual yearly means or individual seasonal means depending on whether we are analyzing annual- or seasonal-mean quantities.

We note that we have also analyzed the data by removing the daily zonal mean instead of defining temporal anomalies, as well as retained the seasonal cycle and interannual variability, and in all cases the results are similar. We present results for December–February (DJF) and June–August (JJA); however, we have also analyzed the shoulder seasons. Results for these seasons depict the atmosphere transitioning between extremes during winter and summer, and are not shown here for brevity.

3. Calculation of eddy length scale

We describe the zonal and meridional lengths of the vorticity anomalies by calculating the *e*-folding lengths of the one-point vorticity correlation plots. This is done by defining a base point (latitude–longitude pair) and correlating the time series of the anomalous vorticity at

the base point with the anomalous vorticity at every grid point on that pressure level. This results in a one-point correlation map centered on the base point. We repeat this calculation for all possible base points (all grid points) and all pressure levels (15 levels from 1000 to 50 mb).

Figure 1 shows the correlation map at (55°N/S, 0°) for the Southern and Northern Hemisphere calculations. The correlations at the anomaly centers are identically equal to one since this represents the correlation of the base point with itself. From this plot alone, it is evident that the Southern Hemisphere vorticity anomalies are larger in the zonal direction than those in the Northern Hemisphere, an observation also made by Chang (1999).

To quantify the size of the anomalies, we slice the correlation plots through the base point and along the zonal and meridional axes (see dashed black lines in Fig. 1). These curves are interpolated to a $0.01° \times 0.01°$ grid, and the average meridional distance and average zonal distance between the base point and the point where the correlations drop below $1/e$ are defined as the vorticity length scale in the meridional and zonal directions, respectively. Near the pole, where the correlations in the meridional direction may never drop to $1/e$, we designate the eddy length as ''not defined.''

Other studies define the eddy length scale as a zonal scale derived from the Fourier decomposition of meridional velocity (Kidston et al. 2010). We have chosen to use correlation *e*-folding lengths instead, as it allows us to easily calculate a meridional scale of the eddies as well as locally define a length scale in sectors of the globe. However, for comparison, we have analyzed vorticity and meridional velocity using Fourier decomposition. To do this, we roughly follow Kidston et al. and calculate the power-weighted average Fourier zonal wavenumber at each latitude:

$$\overline{k}(\theta) = \frac{\sum_k k|\tilde{\mathcal{X}}(k)|^2}{\sum_k |\tilde{\mathcal{X}}(k)|^2}, \tag{1}$$

where $\tilde{\mathcal{X}}$ is the Fourier component of the anomalous vorticity ζ' or meridional wind v'. The Fourier zonal eddy length at each latitude $\overline{\lambda}(\theta)$ is then defined as $2\pi a \cos\theta/\overline{k}(\theta)$, where we only plot results equatorward of 80°N/S to avoid spurious values near the Poles.

4. Results

a. Zonally averaged eddy length scales

Figure 2a shows the zonally averaged correlation *e*-folding lengths of the 200-mb vorticity anomalies ζ' for all days, where the *y* axis denotes both negative and positive latitudes to allow for easy comparison of the two hemispheres. From this figure, it is evident that the vorticity anomalies in the Southern Hemisphere are larger than those in the Northern Hemisphere in both zonal and meridional extent, verifying what was seen in Fig. 1. Performing the same calculations for even and odd years separately results in similar hemispheric differences. Also, in the mid and polar latitudes, the zonal and meridional length scales appear to be similar in both hemispheres, indicating that the vorticity anomalies are isotropic, while in the subtropics and tropics the eddies are zonally elongated.

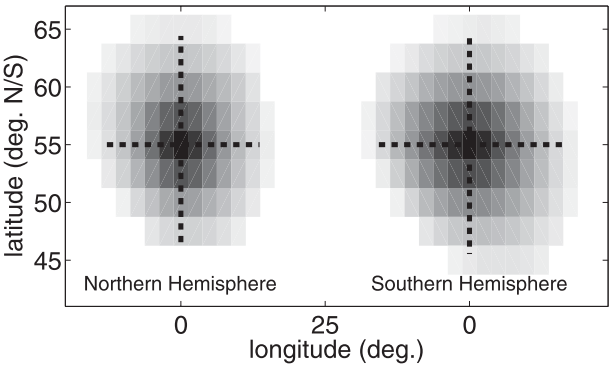

FIG. 1. Example correlation plot at (55°N/S, 0°) of anomalous annual vorticity. The dashed lines denote where the correlations lie above $1/e$ in the zonal and meridional directions. Darker shading denotes larger correlations.

Focusing on the zonal scales, both hemispheres display a peak in zonal eddy vorticity scale near 25°. However, in the midlatitudes, the zonal eddy scale in the Southern Hemisphere is nearly constant, while the zonal lengths of the eddies in the Northern Hemisphere continue to decrease. In the meridional direction, the Southern Hemisphere exhibits a peak in the meridional length of the eddies in the midlatitudes. In the Northern Hemisphere, however, the meridional scale of the eddies gradually increases with latitude at 200 mb with no obvious maximum.

Figure 2b shows the zonally averaged zonal length scales of the vorticity anomalies defined using the Fourier method. The actual lengths are much larger than those calculated using the *e*-folding correlation scale, which is expected since the Fourier scales correspond to an entire wavelength of the wave. To see that the two methods described similar scales, we can explicitly relate the autocorrelation of a cosine wave to its Fourier transform. The autocorrelation and the power spectral density are a Fourier transform pair (Wiener–Khinchin theorem), so the autocorrelation of the cosine wave $Y(x) = \cos(2\pi x/L)$ is $R(x) = \cos(2\pi x/L)$. Thus, we can relate the *e*-folding

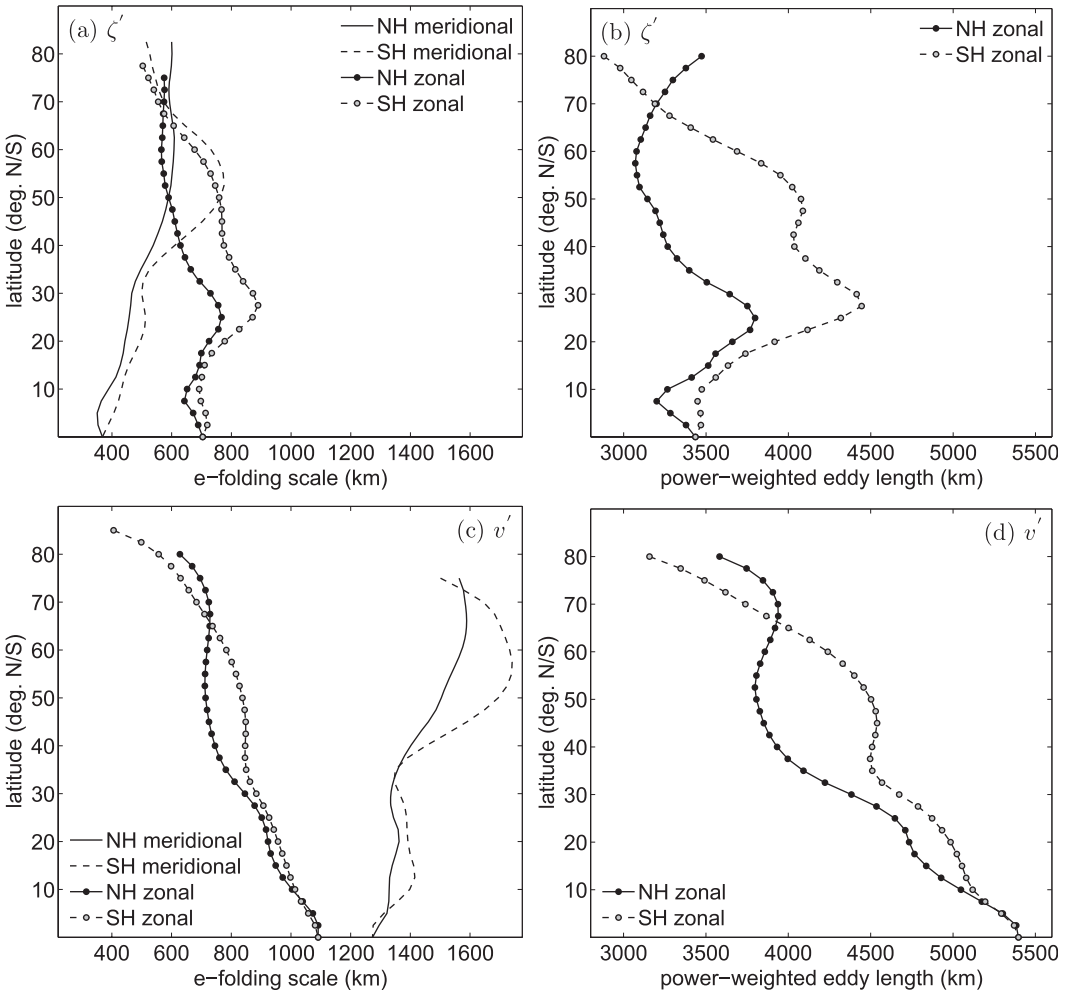

FIG. 2. The 200-mb anomalous annual top vorticity and (bottom) meridional velocity eddy scales calculated using (a),(c) the correlation *e*-folding length averaged around a latitude circle and (b),(d) the average power-weighted Fourier wavenumber.

length scale x_e of the autocorrelation function to the wavelength L by

$$e^{-1} = \cos(2\pi x_e/L); \quad x_e = 0.19L. \tag{2}$$

From Fig. 2b, the maximum Fourier zonal length scale in the Southern Hemisphere is approximately 4500 km. Substituting this into (2) yields a correlation *e*-folding distance of 850 km, very similar to what we see in Fig. 2a. Thus, the Fourier decomposition method yields similar results to those obtained using the correlation method.

We perform the same calculations using the meridional velocity at 200 mb, instead of the relative vorticity, and show the results in Figs. 2c,d. The main difference between the vorticity and meridional velocity results is that the meridional velocity shows much larger meridional length scales compared to vorticity. As with vorticity, the Southern Hemisphere zonal and meridional eddy length scales are larger than those in the Northern Hemisphere in the midlatitudes. In addition, we see similar results to those of Chang (1999), where he found using one-point correlation maps of meridional velocity that the zonal scales of the wave packets decrease toward the poles.

For the rest of this analysis, we focus solely on the length scales of relative vorticity. We choose this variable because it is a scalar quantity that is straightforward to interpret in the context of large-scale dynamics. In addition, recent findings using satellite data show that the cloud scales in the Southern Hemisphere are larger than those found in the Northern Hemisphere (Marchand 2012). In this context, vorticity emphasizes the smaller scales that are more directly associated with precipitation.

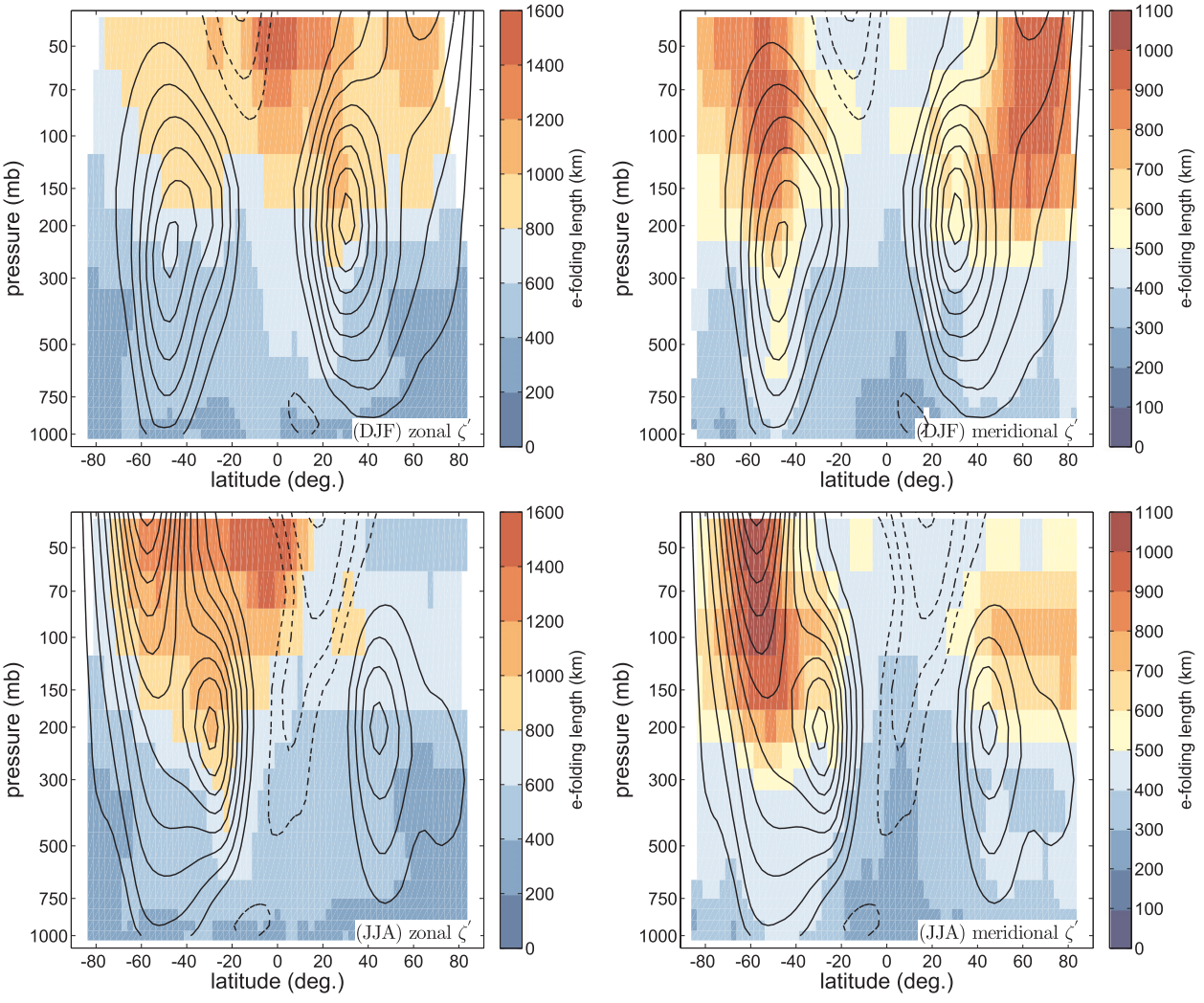

FIG. 3. Correlation *e*-folding lengths of anomalous vorticity in the (left) zonal and (right) meridional direction. The climatological zonal wind is contoured every 5 m s^{-1} with the zero contour omitted and negative values denoted with dashed lines.

b. Pressure–latitude cross sections of seasonal length scales

Figure 3 displays the zonally averaged zonal and meridional DJF and JJA eddy length scales as a function of pressure and latitude. Overlaid on these panels is the seasonal-mean zonal-mean zonal wind. The distributions show a strong seasonal cycle, with each hemisphere displaying its largest length scales during winter. In terms of the vertical distribution, the maximum length scales appear above 150 mb since smaller synoptic scale waves cannot propagate into the stratosphere (Charney and Drazin 1961; Matsuno 1970).

In the winter hemisphere, the zonal scales above 300 mb roughly follow the strongest zonal winds, while below they align with the equatorward flank of the jet. In both DJF and JJA, a band of upper-level easterlies exists near the equator, and the largest zonal scales appear to peak in the winter hemisphere and terminate at the latitude of easterlies in the summer hemisphere.

Interestingly, we see that the largest meridional scales do not necessarily align with the largest zonal scales, but rather they are located in the midlatitude stratosphere, extending downward into the upper troposphere with the largest lengths found in the Southern Hemisphere during JJA.

c. Seasonal length scales on isobaric surfaces

We now present latitude–longitude maps of the correlation length scales. Figure 4 depicts global maps of 200-mb eddy vorticity scales in DJF and JJA. As seen in the zonal average, the distributions show a strong seasonal cycle and the largest zonal scales clearly follow the

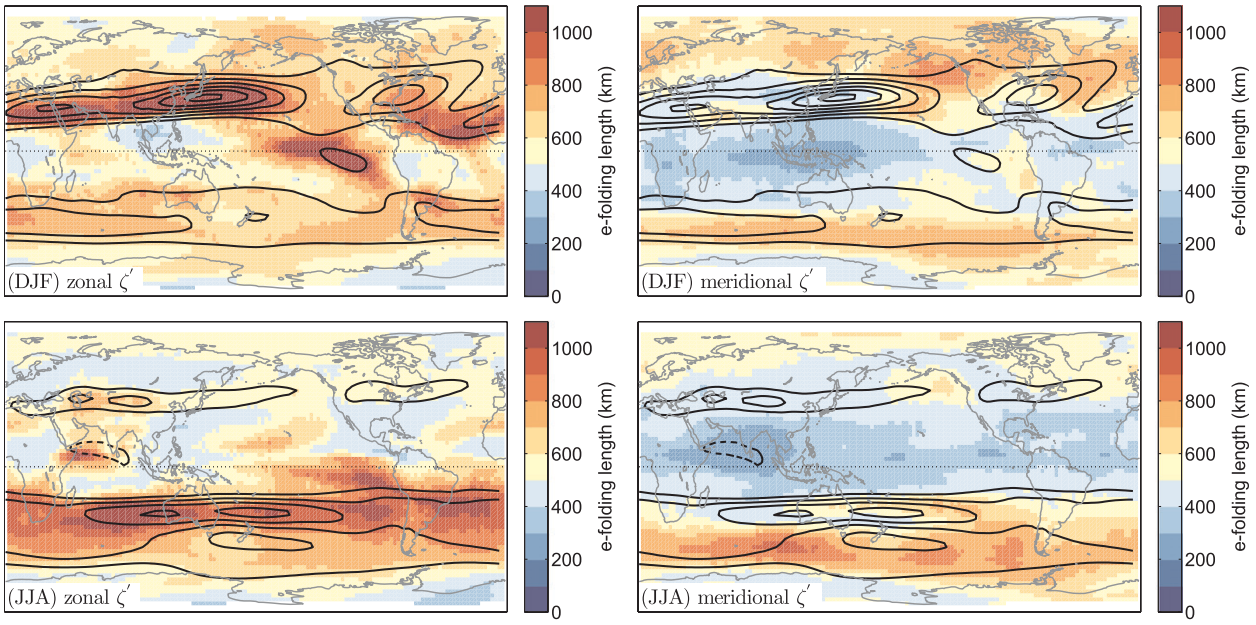

FIG. 4. The 200-mb anomalous vorticity correlation *e*-folding lengths in the (left) zonal and (right) meridional directions. The climatological 200-mb zonal wind is contoured every 10 m s^{-1} starting at ±20 m s^{-1} with negative contours dashed.

strongest zonal winds. The meridional scales do not align with the upper-level jets, but rather the maximum meridional scales tend to occur near the jet exit regions (e.g., the Gulf of Alaska and south of Australia). In addition, the smallest meridional scales appear in the Indian Ocean basin, which is a region of strong easterlies in JJA.

Figure 3 shows that the largest zonally averaged zonal eddy scales appear in the stratosphere, so we plot the length scales at 50 mb in Fig. 5 to give another view of the eddies at upper levels. The meridional scales peak near both poles in DJF and peak near Antarctica in JJA at 50 mb. The largest zonal scales at 50 mb appear along a somewhat zonally symmetric band near the equator, aligning well with the summer hemisphere easterlies.

5. Discussion and conclusions

In this article, we document the climatological distribution of zonal and meridional eddy length scales in DJF and JJA. We find that the Southern Hemisphere exhibits larger eddy scales than the Northern Hemisphere and the maximum zonal eddy scales follow the contours of the strongest zonal winds at upper levels, while the longer meridional length scales tend to peak in the jet exit regions.

The fact that the largest zonal vorticity scales at upper levels follow the strongest zonal winds in the midlatitudes is perhaps not surprising. Consider the zonal phase speed of a Rossby wave linearized about a background zonal flow $\mathcal{U}$:

$$c_{px} = \mathcal{U} - \frac{\beta}{k^2 + l^2}, \tag{3}$$

where k and l are the zonal and meridional wavenumbers of the wave. Rearranging this equation gives

$$(\mathcal{U} - c_{px})(k^2 + l^2) = \beta. \tag{4}$$

Assuming the zonal wind increases more than the phase speed of the wave, if $\mathcal{U}$ increases along a latitude circle (beta is constant), the scale of the wave must increase ($k^2 + l^2$ must decrease). Intuitively, larger scales are required so that planetary vorticity advection may balance larger downstream advection by a stronger mean flow. For this reason, one might expect the largest waves in regions of strong zonal wind, which is indeed what we see in Figs. 3 and 4. Given that the zonal length scales at the jet level appear to follow the zonal wind, that the Southern Hemisphere has larger eddies than the Northern Hemisphere is not surprising since the Southern Hemisphere has stronger climatological zonal winds (Peixoto and Oort 1992).

These findings are consistent with Frierson et al. (2006), where changes in eddy length scales in a simplified GCM were best predicted by the Rhines scale ($\sqrt{v_{\rm rms}/\beta}$), where $v_{\rm rms}$ is the square root of the eddy kinetic energy. On the other hand, since the Rhines scale depends on the eddy

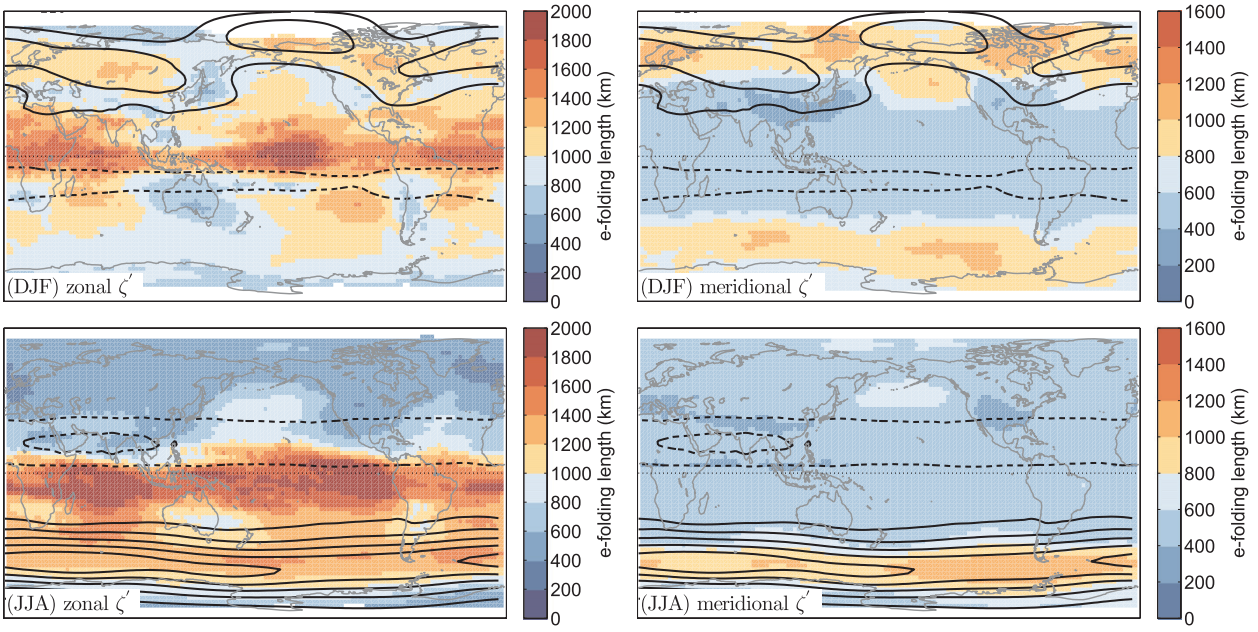

FIG. 5. As in Fig. 4 but at 50-mb. The climatological 50-mb zonal wind is contoured every 10 m s^{-1} starting at ±10 m s^{-1}, with negative contours dashed.

kinetic energy, which is a function of the meridional temperature gradient, it is possible that other baroclinic effects may play a role in determining the seasonal and spatial variations of zonal eddy length. In this case, the strong correlation between the zonal eddy lengths and the zonal winds may not be causal as linear Rossby wave propagation arguments imply. Further work with idealized models is required to determine if either is the dominant mechanism. It is also possible that seasonal and spatial differences in baroclinic instability could, instead, account for the variations in eddy length scales in the upper troposphere. However, Frierson and Davis (2011) analyze the seasonal cycle of static stability and find that over the midlatitude oceans, both the moist and dry static stability decrease during winter, which would imply a decrease in the radius of deformation and thus smaller eddy length scales. We find larger eddies in both hemispheres during winter, which suggests that differences in baroclinicity cannot explain the observed eddy scales.

Although the largest zonal lengths at 200 mb are typically found along the jet stream axes, another peak in eddy length exists near the equator in the Eastern Pacific during DJF (Fig. 4). This region corresponds to a band of equatorial westerlies and has been shown to act as a duct, allowing waves to propagate from one hemisphere to the other (Webster and Holton 1982; Waugh and Polvani 2000; Waugh 2005). One-point correlation maps from this region give evidence of Rossby waves propagating into this region from the extratropics, an example of which is plotted in Fig. 6. Lagged one-point correlation maps also suggest triggering of equatorial waves, which may be related to the development of convection as these vorticity signals reach the deep tropics.

Unlike at 200 mb, the zonal lengths at 50 mb are largest at the equator and abruptly terminate at the edge of the strong band of easterlies in the summer hemisphere (see Figs. 3, 5). These increased eddy length scales are likely evidence of the inertially unstable flow associated with the strong easterlies there. Knox and Harvey (2005) document regions of inertial instability in the lower stratosphere and find that most occurrences are found within 30° of the equator, with the distribution

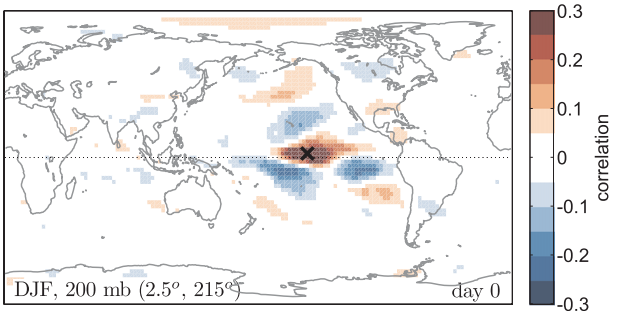

FIG. 6. One-point correlation map of DJF anomalous vorticity at 200 mb with base point (2.5°N, 215°E) denoted by a cross. The color bar denotes correlation, where values greater than (less than) 0.25 (−0.25) are shaded a similar color.

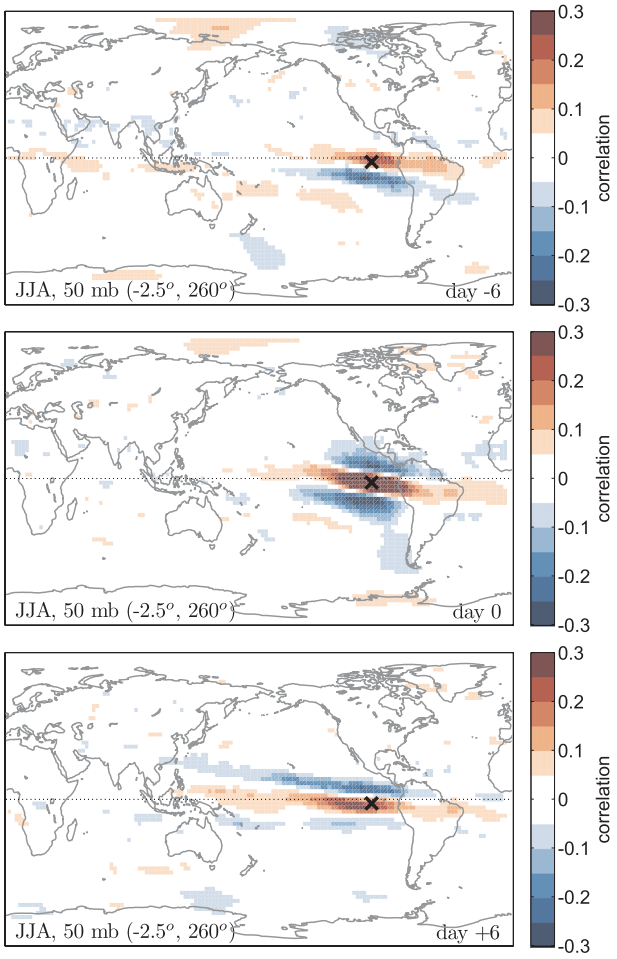

FIG. 7. Lagged one-point correlation maps of JJA anomalous vorticity at 50 mb with base point (2.5°S, 260°E) denoted by a cross. The colorbar denotes correlation, where values greater than (less than) 0.25 (−0.25) are shaded a similar color.

offset into the winter hemisphere and extending around the globe, as we see here. Consistent with the picture of inertial instability generating waves at the equator, lagged one-point correlation plots of anomalous vorticity in this region depict waves that appear to partially develop locally at the equator and then propagate westward, as shown in Fig. 7.

In both hemispheres, on average, the zonal eddy length scales decrease with latitude, while the meridional scales increase slightly with latitude. Basic Rossby wave propagation theory can potentially explain this observation. Imagine a Rossby wave of zero frequency emanating from the midlatitude jet and propagating equatorward, and suppose that $\beta/\overline{u}$ increases toward the low latitudes. Rossby wave tracing on the sphere tells us that the frequency and zonal wavenumber will remain constant during propagation and that the meridional wavenumber will increase to satisfy the Rossby wave dispersion relation (Hoskins and Karoly 1981). In terms of physical eddy lengths, this implies that the zonal length scale will increase and the meridional length will decrease as the wave propagates equatorward. Consistent with this argument, we see that the meridional scales tend to be smallest in the tropical troposphere, while the zonal scales tend to be largest there (see Figs. 2, 3).

This work highlights the relationship between the strong zonal wind and the scale of the eddies, demonstrating that observed eddy vorticity length scales vary regionally and exhibit a clear seasonal cycle. Since the scale of the waves plays a large role in determining their propagation characteristics and ultimate effects on the general circulation, understanding their spatial and seasonal distributions is critical to understanding future circulation changes. These results suggest that a change in wind speed could potentially change the distribution of eddy scales, which through a feedback loop has the potential to affect the wind profiles themselves.

Acknowledgments. We thank the three anonymous reviewers for their helpful comments on an earlier version of this manuscript. This work was supported by the Climate Dynamics Program of the National Science Foundation under Grant AGS-0960497. The ERA-40 global atmospheric reanalysis was provided by ECMWF and is distributed by the Computational Information Systems Laboratory (CISL) at NCAR.

REFERENCES

Barnes, E. A., and D. L. Hartmann, 2011: Rossby wave scales, propagation, and the variability of eddy-driven jets. *J. Atmos. Sci.,* **68,** 2893–2908.

Chang, E. K. M., 1999: Characteristics of wave packets in the upper troposphere. Part II: Seasonal and hemispheric variations. *J. Atmos. Sci.,* **56,** 1729–1747.

—— and D. B. Yu, 1999: Characteristics of wave packets in the upper troposphere. Part I: Northern Hemisphere winter. *J. Atmos. Sci.,* **56,** 1708–1728.

Charney, J. G., and P. G. Drazin, 1961: Propagation of planetary-scale disturbances from the lower into the upper atmosphere. *J. Geophys. Res.,* **66,** 83–109.

Frierson, D. M. W., and N. A. Davis, 2011: The seasonal cycle of midlatitude static stability over land and ocean in global reanalyses. *Geophys. Res. Lett.,* **38,** L13803, doi:10.1029/2011GL047747.

——, I. M. Held, and P. Zurita-Gator, 2006: A gray-radiation aquaplanet moist GCM. Part I: Static stability and eddy scale. *J. Atmos. Sci.,* **63,** 2548–2566.

Hoskins, B. J., and D. J. Karoly, 1981: The steady linear response of a spherical atmosphere to thermal and orographic forcing. *J. Atmos. Sci.,* **38,** 1179–1196.

——, I. N. James, and G. H. White, 1983: The shape, propagation and mean-flow interaction of large-scale weather systems. *J. Atmos. Sci.,* **40,** 1595–1612.

Kidston, J., S. M. Dean, J. A. Renwick, and G. K. Vallis, 2010: A robust increase in the eddy length scale in the simulation of future climates. *Geophys. Res., Lett.,* **37,** L03806, doi:10.1029/2009GL041615.

Knox, J. A., and V. L. Harvey, 2005: Global climatology of inertial instability and Rossby wave breaking in the stratosphere. *J. Geophys. Res.,* **110,** D06108, doi:10.1029/2004JD005068.

Marchand, R. T., 2012: Spatial correlation of hydrometeor occurrence, reflectivity, and rain rate from *CloudSat*. *J. Geophys. Res.,* **117,** D06202, doi:10.1029/2011JD016678.

Matsuno, T., 1970: Veritcal propagation of stationary planetary waves in the winter Northern Hemisphere. *J. Atmos. Sci.,* **27,** 871–883.

Meehl, G. A., C. Covey, K. E. Taylor, T. Delworth, R. J. Stouffer, M. Latif, B. McAvaney, and J. F. B. Mitchell, 2007: The WRCP CMIP3 multimodel dataset: A new era in climate change research. *Bull. Amer. Meteor. Soc.,* **88,** 1383–1394.

Peixoto, J. P., and A. H. Oort, 1992: *Physics of Climate*. Springer Verlag, 520 pp.

Uppala, S. M., and Coauthors, 2005: The ERA-40 Re-Analysis. *Quart. J. Roy. Meteor. Soc.,* **131,** 2961–3012.

Waugh, D. W., 2005: Impact of potential vorticity intrusions on subtropical upper tropospheric humidity. *J. Geophys. Res.,* **110,** D11305, doi:10.1029/2004JD005664.

——, and L. M. Polvani, 2000: Climatology of intrusions into the tropical upper troposphere. *Geophys. Res., Lett.,* **27,** 3857–3860.

Webster, P. J., and J. R. Holton, 1982: Cross-equatorial response to middle-latitude forcing in a zonally varying basic state. *J. Atmos. Sci.,* **39,** 722–733.